Dynamic contrast enhanced MRI for the evaluation of lung perfusion in idiopathic pulmonary fibrosis

Luis A. Torres [1], Kristine E. Lee [2], Gregory P. Barton [1], Andrew D. Hahn [1], Nathan Sandbo [3], Mark L. Schiebler [3,4] and Sean B. Fain [1,4,5,6]

[1]Dept of Medical Physics, School of Medicine and Public Health, University of Wisconsin – Madison, Madison, WI, USA. [2]Dept of Biostatistics and Medical Informatics, School of Medicine and Public Health, University of Wisconsin – Madison, Madison, WI, USA. [3]Dept of Medicine, School of Medicine and Public Health, University of Wisconsin – Madison, Madison, WI, USA. [4]Dept of Radiology, School of Medicine and Public Health, University of Wisconsin – Madison, Madison, WI, USA. [5]Dept of Biomedical Engineering, College of Engineering, University of Wisconsin – Madison, Madison, WI, USA. [6]Dept of Radiology, Carver College of Medicine, University of Iowa, Iowa City, IA, USA.

Corresponding author: Sean B. Fain (sean-fain@uiowa.edu)

Abstract

Background The objective of this work was to apply quantitative and semiquantitative dynamic contrast enhanced magnetic resonance imaging (DCE-MRI) methods to evaluate lung perfusion in idiopathic pulmonary fibrosis (IPF).

Methods In this prospective trial 41 subjects, including healthy control and IPF subjects, were studied using DCE-MRI at baseline. IPF subjects were then followed for 1 year; progressive IPF (IPF_{prog}) subjects were distinguished from stable IPF (IPF_{stable}) subjects based on a decline in percent predicted forced vital capacity (FVC % pred) or diffusing capacity of the lung for carbon monoxide (D_{LCO} % pred) measured during follow-up visits. 35 out of 41 subjects were retained for final baseline analysis (control: n=15; IPF_{stable}: n=14; IPF_{prog}: n=6). Seven measures and their coefficients of variation (CV) were derived using temporally resolved DCE-MRI. Two sets of global and regional comparisons were made: control *versus* IPF groups and control *versus* IPF_{stable} *versus* IPF_{prog} groups, using linear regression analysis. Each measure was compared with FVC % pred, D_{LCO} % pred and the lung clearance index (LCI % pred) using a Spearman rank correlation.

Results DCE-MRI identified regional perfusion differences between control and IPF subjects using first moment transit time (FMTT), contrast uptake slope and pulmonary blood flow (PBF) ($p \leqslant 0.05$), while global averages did not. FMTT was shorter for IPF_{prog} compared with both IPF_{stable} (p=0.004) and control groups (p=0.023). Correlations were observed between PBF CV and D_{LCO} % pred ($r_s = -0.48$, p=0.022) and LCI % pred ($r_s = +0.47$, p=0.015). Significant group differences were detected in age (p<0.001), D_{LCO} % pred (p<0.001), FVC % pred (p=0.001) and LCI % pred (p=0.007).

Conclusions Global analysis obscures regional changes in pulmonary haemodynamics in IPF using DCE-MRI in IPF. Decreased FMTT may be a candidate marker for IPF progression.

Introduction

Idiopathic pulmonary fibrosis (IPF) is a fatal progressive disease affecting approximately 5 million people worldwide [1]. However, the pathology of IPF is difficult to characterise using conventional pulmonary function tests (PFTs) and disease progression is especially difficult to evaluate with current clinical tools. The standard of care for IPF is high-resolution computed tomography (HRCT) for initial diagnosis and often this is accompanied by an invasive histological analysis. Longitudinal monitoring is performed using PFTs, including the change in forced vital capacity (FVC) and diffusing capacity of the lung for carbon

monoxide (D_{LCO}). A significant drop in FVC and D_{LCO} at 6–12 months has been shown to be moderately correlated with disease progression and mortality [2, 3]. However, these are global lung measurements that might be insensitive to subtle regional changes in IPF. Additionally, significant progression of the disease must occur before changes in HRCT, FVC and D_{LCO} are detectable, reducing their overall clinical prognostic value [4]. Consequently, improved biomarkers for accurate monitoring and early detection of IPF progression are needed.

Pulmonary magnetic resonance imaging (MRI) is a promising technique with the ability to provide longitudinal and regional information on pulmonary function [5]. Spatially resolved pulmonary perfusion is typically evaluated using dynamic contrast enhanced MRI (DCE-MRI), although various noncontrast methods are increasingly applied. DCE-MRI can provide quantitative and semiquantitative measures, and has been used to explore pulmonary haemodynamics in healthy and diseased subjects [6–10]. Despite the growing use of pulmonary contrast enhanced MRI, prior work in IPF is not extensive and most research focuses on semiquantitative analysis [11–15]. To the best of our knowledge, there are no fully quantitative estimates of pulmonary haemodynamics in IPF using DCE-MRI techniques.

Quantitative measures based on indicator dilution methods [16] provide physiological estimates of pulmonary blood flow (PBF), pulmonary blood volume (PBV) and mean transit time (MTT) [17–19], while semiquantitative measures are characteristics of the contrast enhancement time-series such as contrast time of arrival (TOA), time to peak (TTP), first moment transit time (FMTT), full width at half maximum (FWHM) [14] and wash-in slope (SLOPE) [10]. Advantages of more quantitative measures such as PBF, PBV and MTT are offset by challenges in obtaining accurate measures of the arterial input function (AIF), increased computational complexity and longer scan times required to obtain enough data to solve the ill-posed problem. Consequentially this leads to longer sustained breath-holds and increased potential for motion corruption. This makes accurate quantitation especially difficult in severely diseased or noncompliant subjects (*e.g.* paediatric subjects) who have a significant imaging failure rate. Alternatively, semiquantitative measures are simpler to compute and require fewer temporal phases. This can improve the chances of successful imaging, albeit without the advantages of consistent haemodynamic physiological interpretation.

The objective of this work was to develop quantitative and semiquantitative DCE-MRI methods for application in IPF. We hypothesised DCE-MRI could be used to detect global and regional perfusion differences between IPF and healthy ageing volunteers. In an exploratory analysis we also followed IPF subjects for 1 year clinically to monitor progression; we hypothesised there would be differences in perfusion measures in a progressive subgroup of IPF (IPF$_{prog}$) compared with a stable subgroup of IPF (IPF$_{stable}$) and with healthy ageing volunteers. We tested these hypotheses using a repeated measures linear regression analysis to adjust for demographic and technical factors found to be significant covariates. Furthermore, we hypothesised our measures of haemodynamics would correlate with clinical PFTs used to monitor IPF progression, specifically FVC, D_{LCO} and the lung clearance index (LCI), a measure of ventilation heterogeneity.

Methods

Study population

Our Health Insurance Portability and Accountability Act-compliant and Institutional Review Board-approved (UW IRB 2013-0266 and UW IRB 2014-1572) prospective study included 41 subjects imaged longitudinally (two to four visits) from 2015 to 2020 using DCE-MRI at the School of Medicine and Public Health, University of Wisconsin – Madison (Madison, WI, USA). Written and informed consent was obtained from all subjects. Healthy subjects were included for study if >18 years of age, current nonsmoker and no history of cancer or heart disease. The healthy subject population was deliberately enriched for individuals aged >50 years and 65% male sex to better match the age and sex distribution of the recruited IPF population. IPF subjects required age >18 years with clinical diagnosis of IPF and no recent exacerbations. Exclusion criteria consisted of MRI contraindication, pregnancy/lactation or any medical condition that could interfere with the ability to comply with the protocol. IPF$_{prog}$ were distinguished from IPF$_{stable}$ subjects by a >10% decline in FVC % pred or a >15% decline in D_{LCO} % pred 1 year after baseline PFT measures. For this feasibility study we limit analysis to the first visit passing quality control for each subject and leave longitudinal analysis for a subsequent report. Subject attrition during the study is summarised in supplementary table S1. Specifically, two stable IPF subjects withdrew during their first visit due to claustrophobia, while technical failure occurred in four more subjects (one healthy and three progressive IPF) due to either loss of breath-hold during the scan or delayed arrival of contrast agent leading to truncation of the contrast kinetic curve; these subject scans were omitted from analysis based on the number of frames of washout data obtained in the AIF. Each image series was

visually inspected and excluded if there was a loss of breath-hold. If a subject's initial baseline visit failed quality control, a subsequent passing baseline visit was used in its place. In total, 35 out of 41 subjects were included for analysis (healthy control: n=15, five males, age 56.3±14.2 years; IPF$_{stable}$: n=14, 12 males, age 69.9±9.3 years; IPF$_{prog}$: n=6, five males, age 75.7±4.4 years). Descriptive statistics and intragroup comparisons for the 35 subjects included in the analysis are provided in table 1.

Acquisition and reconstruction protocol

Subjects were scanned while supine at end-expiratory breath-hold. Contrast injection was performed using a dose of 0.05 mmol·kg^{-1} gadobenate dimeglumine (Gd-BOPTA, MultiHance; Bracco Imaging, Monroe Township, NJ, USA) at 4 mL·s^{-1} followed by a 35 mL saline flush to approximate a linear relationship between signal intensity and contrast concentration in the lung parenchyma [20].

Due to hardware upgrades during the study, subjects were imaged at both 1.5 and 3 T field strengths. DCE pulmonary perfusion scans were acquired using three-dimensional spoiled gradient-echo sequences. Similar sampling schemes were used for time-resolved acquisition at each field strength, including a research pulse sequence, "interleaved variable density" [21] at 1.5 T (Signa HDxt; GE Healthcare, Chicago, IL, USA), and a commercial pulse sequence, "DIfferential Subsampling with Cartesian Ordering" (DISCO; GE Healthcare) [22] at 3 T (Discovery MR750; GE Healthcare). Both sequences were acquired with full chest coverage, i.e. field of view=40 (superior/inferior)×28 (anterior/posterior)×40 (left/right) cm^3 and a parallel acceleration factor of 2×2. Spatial (4 mm isotropic) and temporal (nominally 1 s) resolutions were matched for each protocol. Other relevant scan parameters are provided in table 2.

TABLE 1 Population characteristics: healthy controls and idiopathic pulmonary fibrosis (IPF) subjects						
	Control (n=15)	IPF$_{stable}$ (n=14)	IPF$_{prog}$ (n=6)	p-value[#]		
				Control versus IPF$_{stable}$	Control versus IPF$_{prog}$	IPF$_{stable}$ versus IPF$_{prog}$
3.0 T						
n (%)	3 (20.0)	6 (42.9)	3 (50.0)	0.735	0.872	1.000
Female						
n (%)	10 (66.7)	2 (14.3)	1 (16.7)	0.023*	0.190	1.000
Age (years)						
Median (IQR)	63.0 (51.5–66.0)	69.0 (64.0–74.0)	75.5 (72.5–79.3)	0.020*	0.002*	0.320
D_{LCO} % pred						
Median (IQR)	94.0 (72.8–105.5)	57.0 (54.0–67.0)	46.0 (45.0–50.0)	0.006*	0.013*	0.090
n (%)	8 (53.0)	13 (92.8)	5 (83.3)			
FVC % pred						
Median (IQR)	105.0 (94.0–109.0)	85.5 (75.8–92.8)	66.5 (57.5–74.8)	0.050*	0.005*	0.062
n (%)	9 (60.0)	14 (100.0)	6 (100.0)			
LCI % pred						
Median (IQR)	7.4 (7.2–7.6)	7.7 (7.5–7.9)	8.0 (7.9–8.125)	0.068	0.025*	0.385
n (%)	8 (53.0)	12 (75.0)	4 (66.7)			
PBF (mL·100 mL^{-1}·min^{-1})						
Median (IQR)	189.0 (142.6–214.3)	155.8 (134.1–193.0)	203.47 (185.0–216.2)	0.978	1.000	0.447
PBV (mL·100 mL^{-1})						
Median (IQR)	16.4 (12.4–18.3)	13.7 (13.1–14.2)	14.7 (12.1–15.8)	1.000	1.000	1.000
MTT (s)						
Median (IQR)	5.6 (5.3–5.8)	5.2 (4.6–6.8)	5.3 (5.2–5.7)	1.000	1.000	1.000
SLOPE (AU)						
Median (IQR)	1.3 (1.2–1.9)	1.3 (0.8–1.8)	1.3 (1.1–1.4)	0.716	1.000	1.000
FMTT (s)						
Median (IQR)	12.9 (12.4–13.3)	13.2 (12.9–16.3)	13.1 (12.2–13.4)	0.231	1.000	0.796
TOA (s)						
Median (IQR)	0.7 (0.2–0.9)	0.9 (0.7–1.5)	0.6 (0.3–0.8)	0.181	1.000	0.323
TTP (s)						
Median (IQR)	5.2 (4.8–5.7)	5.9 (5.5–8.3)	5.8 (5.3–6.2)	0.108	1.000	1.000

IPF$_{stable}$: stable IPF; IPF$_{prog}$: progressive IPF; IQR: interquartile range; D_{LCO}: diffusing capacity of the lung for carbon monoxide; FVC: forced vital capacity; LCI: lung clearance index; PBF: pulmonary blood flow; PBV: pulmonary blood volume; MTT: mean transit time; SLOPE: wash-in slope; AU: arbitrary units; FMTT: first moment transit time; TOA: time of arrival; TTP: time to peak. [#]: numerical values tested using the Wilcoxon rank sum test, categorical values tested using Fisher's exact test. p-values adjusted via the Bonferroni method using three comparisons. *: p<0.05.

TABLE 2 Imaging parameters

	IVD	DISCO
TR (ms)	2.2	2.3
TE (ms)	0.7	0.7
Flip angle (°)	25	30
FOV (mm^3)	400×280×400	400×280×400
Acquisition matrix	100×70×400	100×70×400
Acquired voxel size (mm^3)	4.0×4.0×4.0	4.0×4.0×4.0
Acceleration factor (R)	2	2
Acquired time frames	23	27
Scan length (s)	21	31
Bandwidth (kHz)	125	125
Subjects (n)	23	12

IVD: interleaved variable density; DISCO: DIfferential Subsampling with Cartesian Ordering; TR: repetition time; TE: echo time; FOV: field of view.

Post-processing

Semiautomatic lung segmentation and AIF selection

Segmentation was performed using a combination of ITK-SNAP version 3.8 [23] and Python version 3.6 (www.python.org). Consecutively acquired morphological images were used to semiautomatically segment the perfusion datasets similar to KOHLMANN *et al.* [24]. Each lung was segmented into six regions by volume. An example can be seen in supplementary figure S1. To remove potential user error in AIF selection, we implemented an automated method where we apply successive image processing steps to our dynamic images to gradually isolate the pulmonary trunk and pinpoint its branching point [25]. Additionally, a cross-correlation analysis with the AIF was performed to suppress large vessel influence [26]. A visualisation of these steps is included in supplementary figure S2 and a more detailed description of these methods is included in the supplementary material. Because subjects with extreme motion are excluded from this analysis, we do not apply additional image registration on the DCE time-series.

Quantitative and semiquantitative measures

PFTs (FVC % pred, D_{LCO} % pred and LCI % pred) were performed prior to the DCE-MRI scans, on the same day of each visit, with a MasterScreen PFT system (BD, San Diego, CA, USA) using reference values computed as recommended by the Global Lung Function Initiative [27]. The computation of each measure was performed using MATLAB (R2018b; MathWorks, Natick, MA, USA). Supplementary figure S3 outlines the workflow for computing quantitative and semiquantitative measures as well as example parametric maps in a healthy subject. Voxel-wise relative enhancement was computed *via* subtraction of and normalisation to the baseline mask signal. Using the principles of indicator dilution theory, we can solve for PBF, PBV and MTT. Specifically, the following relationships hold under a few basic assumptions [16]:

$$C(t) = \text{PBF}[R(t) \otimes \text{AIF}] \tag{1}$$

$$\text{PBV} = \frac{\int C(t)\mathrm{d}t}{\int \text{AIF}(t)\mathrm{d}t} \tag{2}$$

$$\text{MTT} = \frac{\text{PBV}}{\text{PBF}} \tag{3}$$

Here $C(t)$ and $R(t)$ are the concentration at the volume of interest and the tissue residue function at time t, respectively. The main task here is to deconvolve eq. 1 to solve for PBF×$R(t)$. This is an ill-posed problem that requires regularisation to reach physiologically plausible solutions [19, 28]. Once PBF×$R(t)$ is computed we solve for PBV and MTT using eqs 2 and 3. In this work PBF, PBV and MTT were estimated by solving a least squares deconvolution problem with Tikhonov regularisation [16, 29, 30]. Details on the deconvolution procedure are included in the supplementary material. Semiquantitative parameters are conceptually simpler to compute. The contrast kinetic curves were smoothed using a second-order Savitsky–Golay filter with a window size of 5 frames. Each time-series was upsampled by a factor of 2 using linear interpolation. TOA and TTP were defined as the time-point at which the signal enhancement curve reaches 20% and 100% of its peak value, respectively. The TTP of the AIF was subtracted from

TOA and TTP to remove potential bolus injection timing differences across subjects. Finally, SLOPE and FMTT were calculated:

$$\text{SLOPE} = \frac{S(\text{TTP}) - S(\text{TOA})}{\text{TTP} - \text{TOA}} \tag{4}$$

$$\text{FMTT} = \frac{\int S(t) * t\, dt}{\int S(t)\, dt} \tag{5}$$

Here $S(\text{TTP})$ is the peak signal and $S(\text{TOA})$ is the baseline signal at TOA. For a visual example of how these parameters are associated with the contrast kinetics, see supplementary figure S4.

Statistical analysis

Comparison of characteristics between controls, $\text{IPF}_{\text{stable}}$ and IPF_{prog} was done using nonparametric tests (Wilcoxon rank sum test for numeric variables and Fisher's exact test for categorical variables) for every pairwise comparison ($\text{IPF}_{\text{stable}}$ with controls, IPF_{prog} with controls and $\text{IPF}_{\text{stable}}$ with IPF_{prog}). A Bonferroni p-value correction using n=3 comparisons was applied to account for multiple-comparisons bias.

We evaluated relationships to each DCE measure on both the whole-lung and a region-specific level. Linear regression models were used to evaluate the relationship of cohort to the whole-lung DCE measure. For region-specific DCE measures, each subject has 12 measures consisting of six regions (three anterior and three posterior) for both the right and left lung. Repeated measures linear regression was performed where correlations between observations within a subject were modelled using an unstructured covariance matrix. Potential simplifications of the variance–covariance structure were assessed using Akaike's Information Criterion. The most parsimonious model considering cohort, region (six levels) and lung (left or right) as well as potential interactions was identified and was similar for most measures. The final parameter estimates were obtained using the restricted maximum likelihood. Model effects for the six-level region and two-level "side" (left or right lung) were evaluated, and only the region effect improved the fit and was retained for the final models. Thus, the final models for region-specific DCE measures included terms for cohort, region, the interaction and between cohort and region.

For each DCE measure, we separately evaluated the mean in the appropriate area (whole-lung or region-specific) and their coefficients of variation (CV) (mean/SD for the whole lung or for the specific region). All models adjusted for sex (two levels: female *versus* male), age (continuous) and field strength (two levels: 1.5 *versus* 3 T). Cohort was evaluated separately as a three-level factor with controls (as the referent group) and $\text{IPF}_{\text{stable}}$ and IPF_{prog}, but also as a two-level factor with $\text{IPF}_{\text{stable}}$ and IPF_{prog} considered together as "IPF". Normality of each DCE measure was evaluated visually and because each measure has a different range they were rescaled to a z-score for comparisons.

Least squares means and 95% confidence intervals with adjustment for age, sex and field strength were estimated for the relevant cohort and region levels. For the whole-lung analysis this consists of cohort; for region-specific analysis this consists of cohort and region interaction. The whole-lung analysis reports the p-value for the cohort comparison. The region-specific analysis reports the p-value for the interaction term as well as the joint likelihood ratio test to get the marginal "overall cohort" (cohort+cohort×region) and "overall region" (region+region×cohort) effects, which represent overall impact of cohort or region.

Spearman correlations were evaluated to compare each DCE-MRI measure with FVC % pred, D_{LCO} % pred and LCI % pred. All analyses were performed in SAS version 9.4 (SAS Institute, Cary, NC, USA) and R (www.r-project.org).

Results

Global lung averages did not differ significantly between IPF and control subjects, even after adjusting for age, sex and field strength (figure 1a); however, regional comparisons showed significant differences between IPF and healthy control subjects for mean PBF, SLOPE and FMTT measures ($p \leqslant 0.05$) (figure 2). For each metric we saw significant cohort, lung region and interaction effects. No statistical differences were found between the left and right lungs; thus, the left and right lungs were grouped into apical (upper), middle and basal (lower) lung regions for both posterior and anterior. Similar variations between lung regions were seen in all measures irrespective of cohort. Regional heterogeneity patterns were also captured across lung regions and cohorts using the CV, in which significant cohort differences were observed for PBF, TTP and FMTT ($p \leqslant 0.05$) (figure 3).
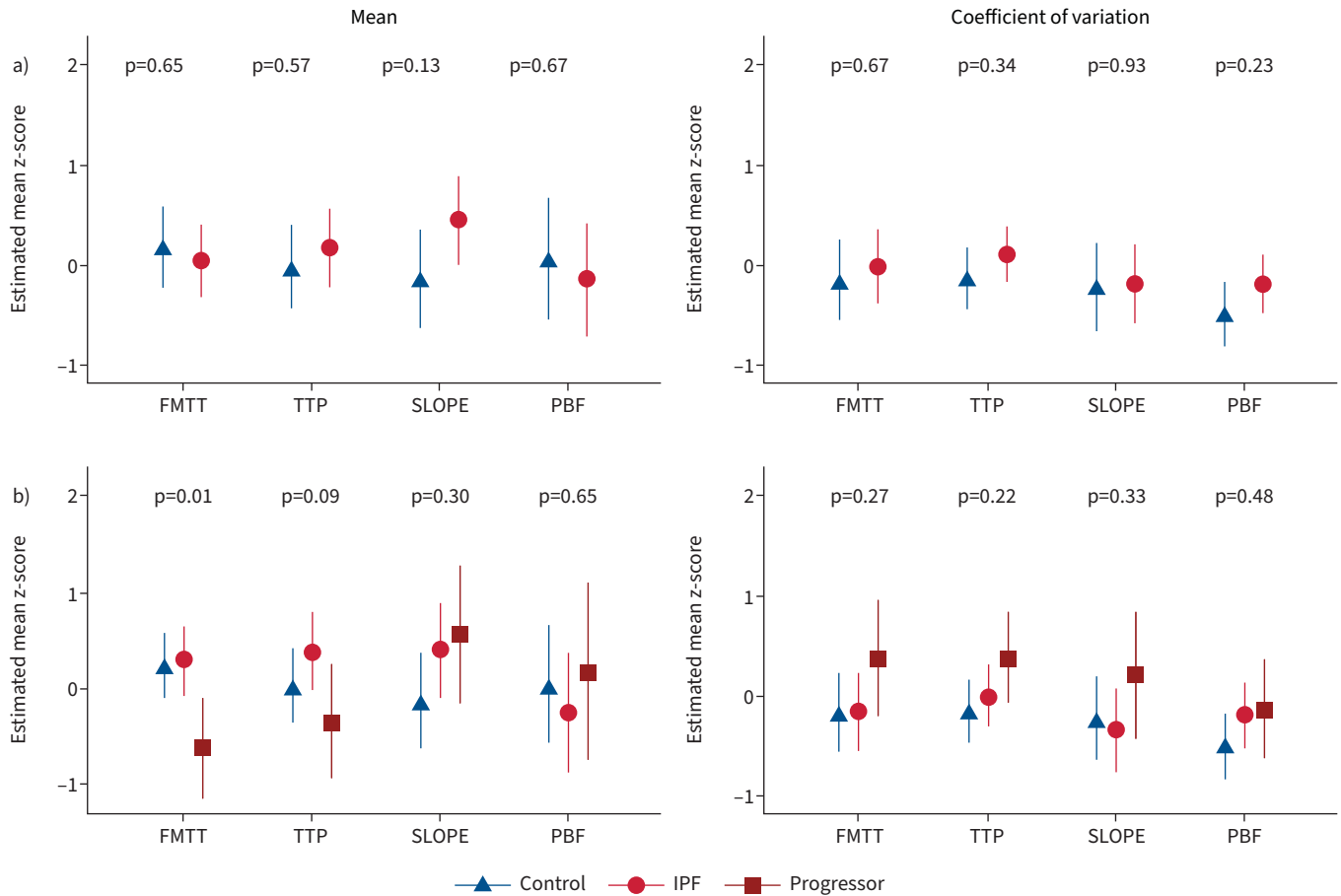
FIGURE 1 Whole-lung linear regression model results for cohort means (left) and coefficients of variation (right) of first moment transit time (FMTT), time to peak (TTP), contrast uptake slope (SLOPE) and pulmonary blood flow (PBF). a) Healthy controls *versus* a combined idiopathic pulmonary fibrosis (IPF) cohort. b) Healthy controls *versus* stable IPF *versus* progressive IPF.

A subset of exemplary parametric maps in two healthy and two IPF subjects is highlighted in figure 4. We observed whole-lung and regional abnormalities in IPF relative to healthy subjects, including increased heterogeneity (CV) of perfusion measures. In healthy control subjects the expected gravity-dependent anterior–posterior gradient pattern predominates, while in IPF subjects additional interpatient and regional spatial variations in severity of perfusion abnormalities were typical. For example, in IPF subject 1 reduced global perfusion is observed, while in IPF subject 2 regional variation in perfusion between the apical and basal lung regions are prominent compared with healthy subjects. A more complete set of parametric maps can be seen in supplementary figure S5.

Further exploratory comparisons of control *versus* IPF_{prog} and IPF_{stable} found global and regional differences in semiquantitative perfusion measures. The global mean FMTT was shorter in IPF_{prog} relative to healthy (p=0.023) and IPF_{stable} groups (p=0.004) (figure 1b). No other measures showed global differences between groups. Regional analysis for these cohorts showed similarly significant differences for control *versus* IPF_{stable} for FMTT (p=0.030) and control *versus* IPF_{prog} for FMTT (p=0.036), where FMTT was shorter in IPF_{prog} (figure 5). Of potential importance for discriminating progression from stable disease, TTP (p=0.032) and FMTT (p<0.001) were both shorter in IPF_{prog} *versus* IPF_{stable}. Similarly, the FMTT CV differed within regions for IPF_{prog} *versus* controls (p=0.034), and importantly, the FMTT CV differed between IPF_{prog} and IPF_{stable} (p=0.002) (figure 6).

Finally, the regional heterogeneity of perfusion measures as measured by the CV was significantly correlated to PFTs. There was mild/moderate correlation between the PBF CV *versus* D_{LCO} % pred (r_s= −0.48, p=0.022) and LCI % pred (r_s= +0.47, p=0.015). No other perfusion measures were found to correlate to PFTs. Significant group differences were detected in age, D_{LCO} % pred, FVC % pred and LCI % pred (p<0.05).
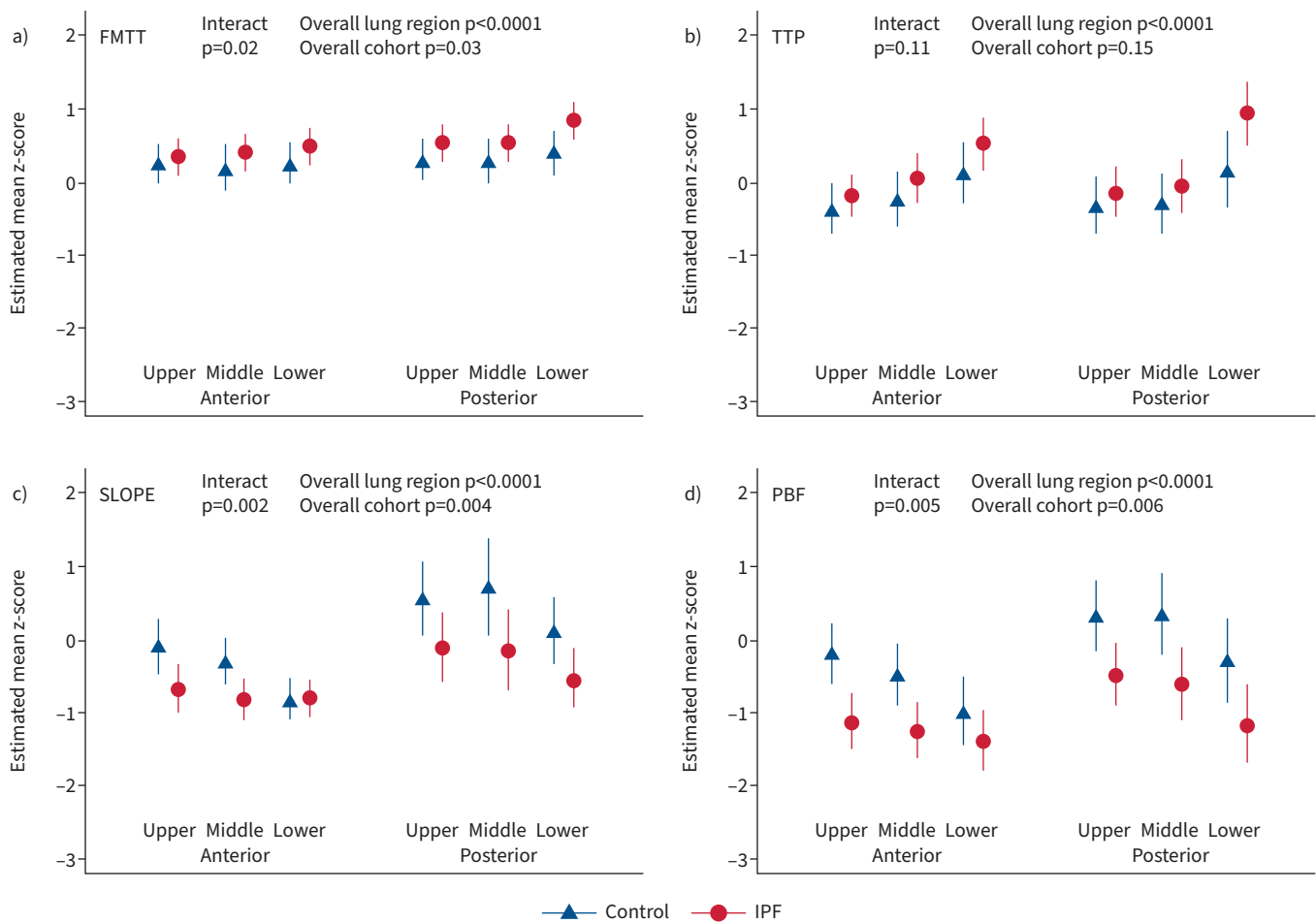
FIGURE 2 Regional repeated measure regression model results for the mean values of a) first moment transit time (FMTT), b) time to peak (TTP), c) contrast uptake slope (SLOPE) and d) pulmonary blood flow (PBF) in healthy control and combined idiopathic pulmonary fibrosis (IPF) subjects.

Discussion

DCE-MRI identified regional perfusion differences between control and IPF lung disease subjects using FMTT, SLOPE and PBF, although global lung averages did not. Heterogeneity in these measures using the CV was also greater in IPF. This suggests global analysis obscures regional changes in pulmonary haemodynamics and highlights the need for regional imaging approaches. Generally, we see increased FMTT and decreased PBF and SLOPE in IPF relative to control subjects, consistent with reports of vascular pruning and overall reduction of vascular density in severely fibrotic areas [31–34]. The increased CV of FMTT, TTP and PBF represent increased regional heterogeneity in IPF relative to healthy control subjects, also consistent with reports of spatially heterogenous vascular remodelling in IPF [33].

There were significant regional variations and trends in all DCE measures consistent with gravitational dependence and previously published works [17, 35]. This pattern is likely related to the supine patient orientation within the MRI scanner, and residual anatomical and physiological effects of upright posture. Additionally, we found larger group discrepancies in the posterior-basal portions of the lungs in all measures and the CV supported more pronounced perfusion differences in these areas, consistent with typical manifestations of IPF [36, 37].

Interestingly, in our exploratory analysis we observed a global decrease in FMTT between IPF$_{prog}$ and both the IPF$_{stable}$ and healthy control groups, but no differences were observed between the control and IPF$_{stable}$ groups, suggesting decreased FMTT may be a candidate marker for progression. One explanation for the shorter FMTT in the IPF$_{prog}$ group is increased regional heterogeneity of vascular density and central vessel diameter due to vascular pruning and remodelling. EBINA et al. [31] found that acute exacerbation, a severe and often fatal adverse event associated with rapid progression, was associated with increased and
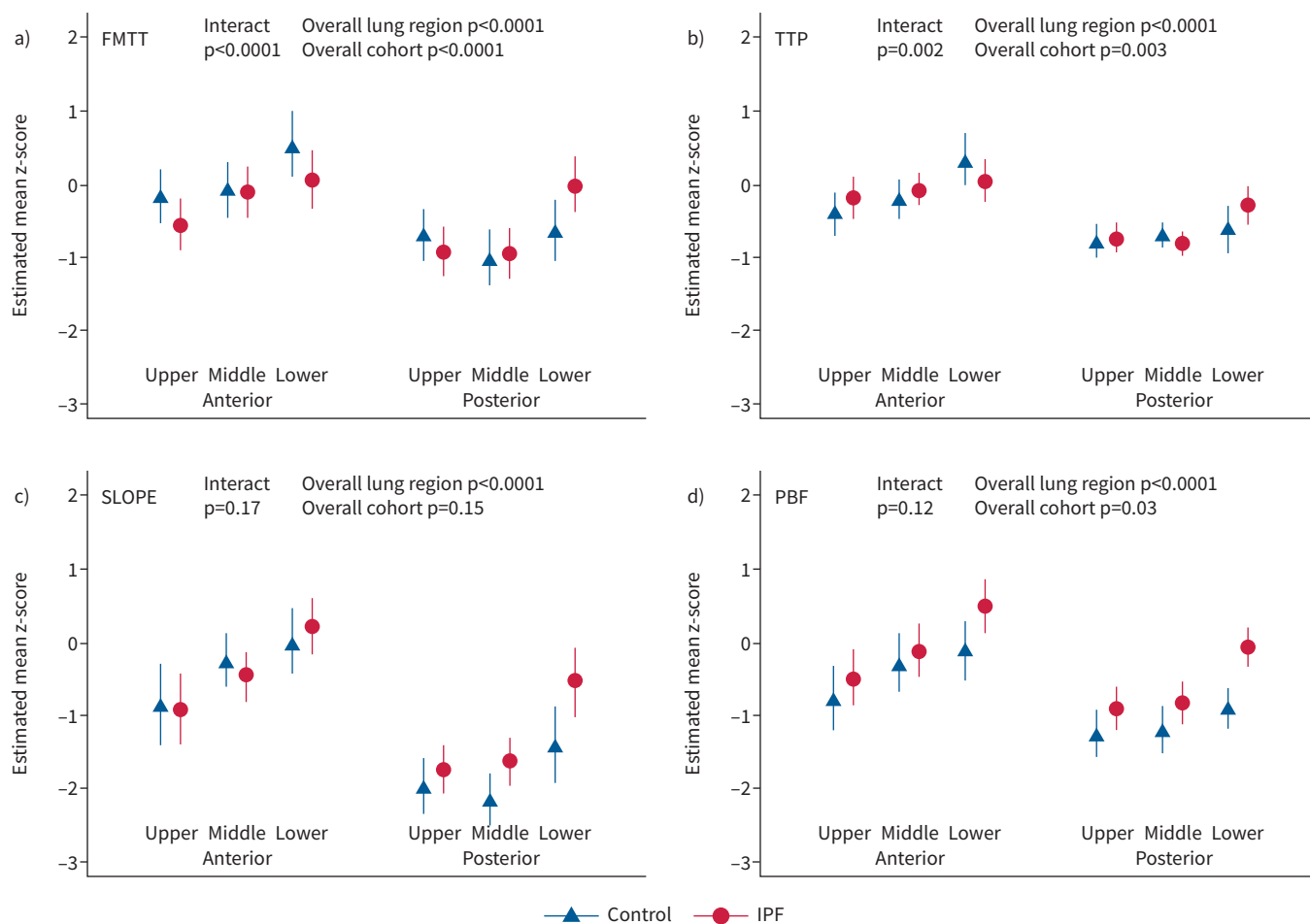
FIGURE 3 Regional repeated measure regression model results for the coefficients of variation of a) first moment transit time (FMTT), b) time to peak (TTP), c) contrast uptake slope (SLOPE) and d) pulmonary blood flow (PBF) in healthy control and combined idiopathic pulmonary fibrosis (IPF) subjects.

dilated capillaries. Similarly, a CT-based vessel analysis found increased vessel size to be highly predictive of mortality [38]. IPF manifests as a heterogeneous fibrotic injury, and is predominantly found in the basal and peripheral portions of the lungs [36, 37]; previous work with DCE-MRI indicates that changes can be detected easier in these areas [14, 15]. It is thought that repetitive environmental microinjuries to interstitial and vascular tissue induce abnormal healing responses which result in heterogeneous interstitial and vascular remodelling [36, 39]. Early results had seemingly conflicting reports of reduced/increased vascular density in IPF. However, this was later reconciled with studies on the spatial heterogeneity of the disease and evidence supports that severely fibrotic areas demonstrate a reduction in vascular density, while adjacent tissues display an increase in vascularisation [31]. Although the mechanism and causality of the increased vascularisation and fibrogenesis is unclear, some authors suggest it is a precursor to fibrosis [40, 41]. Additionally, increased vascularisation and vessel diameter have also been implicated in acute exacerbations in IPF, which lead to rapid progression of fibrosis and result in higher mortality rates [31]. Accurate, regional evaluation of pulmonary microvasculature could provide insight into the pathogenic process of IPF, and these exploratory results warrant further study in a larger population to determine if FMTT remains a possible predictor of progression and to inform on the possible underlying mechanism driving shorter FMTT.

With regard to comparisons with PFTs, including FVC % pred, D_{LCO} % pred and LCI % pred, we observed somewhat unanticipated findings of nonsignificant and universally weak correlation associations with the mean values of all perfusion measures. Although there were moderate correlations of D_{LCO} % pred and LCI % pred with measures of perfusion heterogeneity, no correlations of any perfusion measures
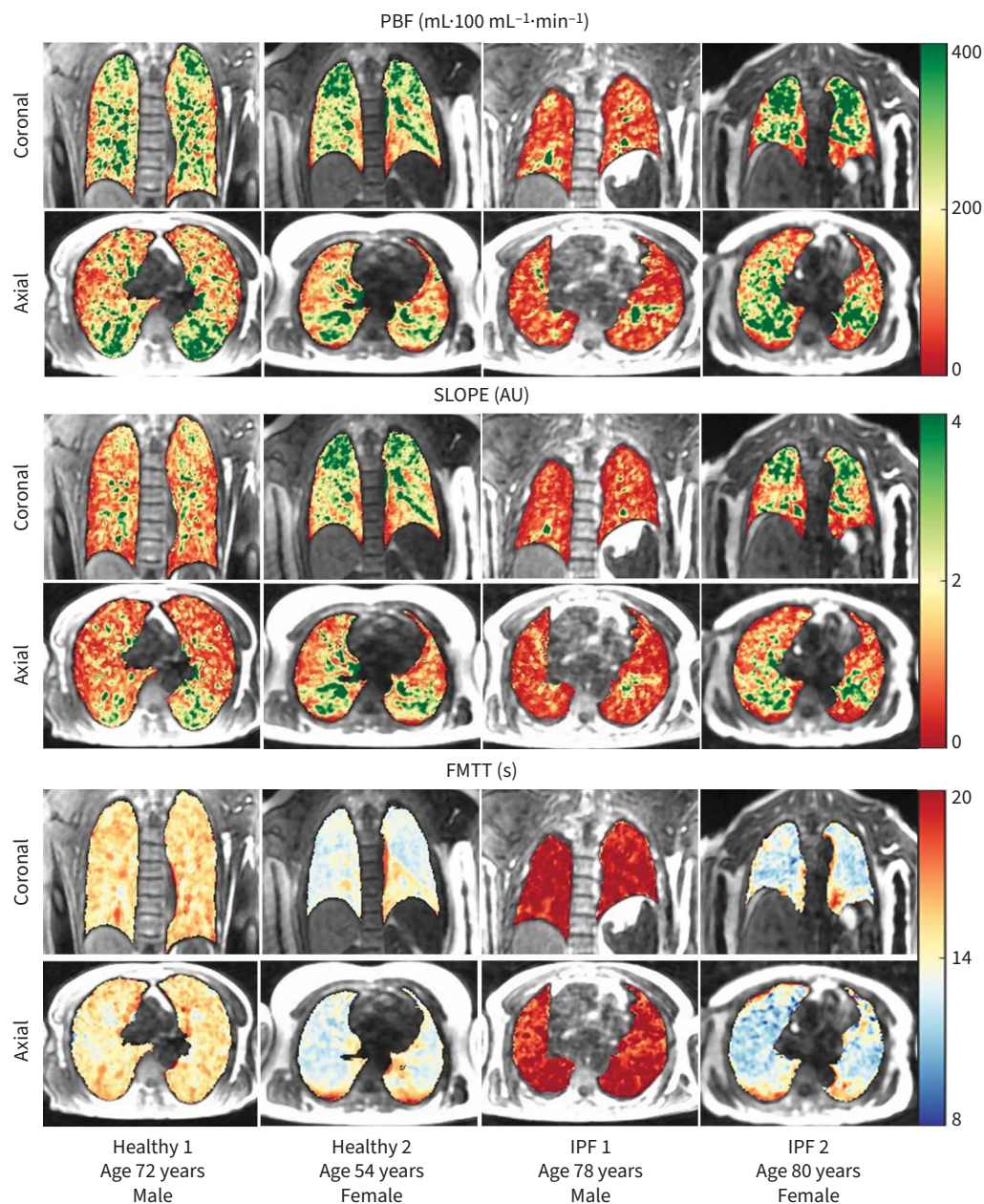
FIGURE 4 A subset of exemplary parametric maps of pulmonary blood flow (PBF), contrast uptake slope (SLOPE) and first moment transit time (FMTT) in two healthy and two idiopathic pulmonary fibrosis (IPF) subjects. For PBF and SLOPE, green and red colours indicate more and less perfusion, respectively. For FMTT, blue and red colours indicate faster and slower transit times, respectively. We observe whole-lung and regional abnormalities in IPF relative to age-matched healthy subjects. Regional heterogeneity of perfusion measures is observed in all subjects. An anterior–posterior gradient is observed in addition to reduced perfusion in the distal portions of the lungs. In IPF subjects, interpatient as well as regional variation in severity is observed.

were observed with FVC % pred. The explanation for this pattern probably lies in heterogeneous compensatory increases in pulmonary perfusion to offset lung function decline. WEATHERLY *et al*. [14] report similar results in which D_{LCO} % pred was not correlated with the contrast curve FWHM, yet D_{LCO} % pred was correlated with the FWHM interquartile range, a measure of regional heterogeneity. This heterogeneity is one reason why IPF is difficult to evaluate and further emphasises the value of spatially resolved functional lung imaging in this disease.
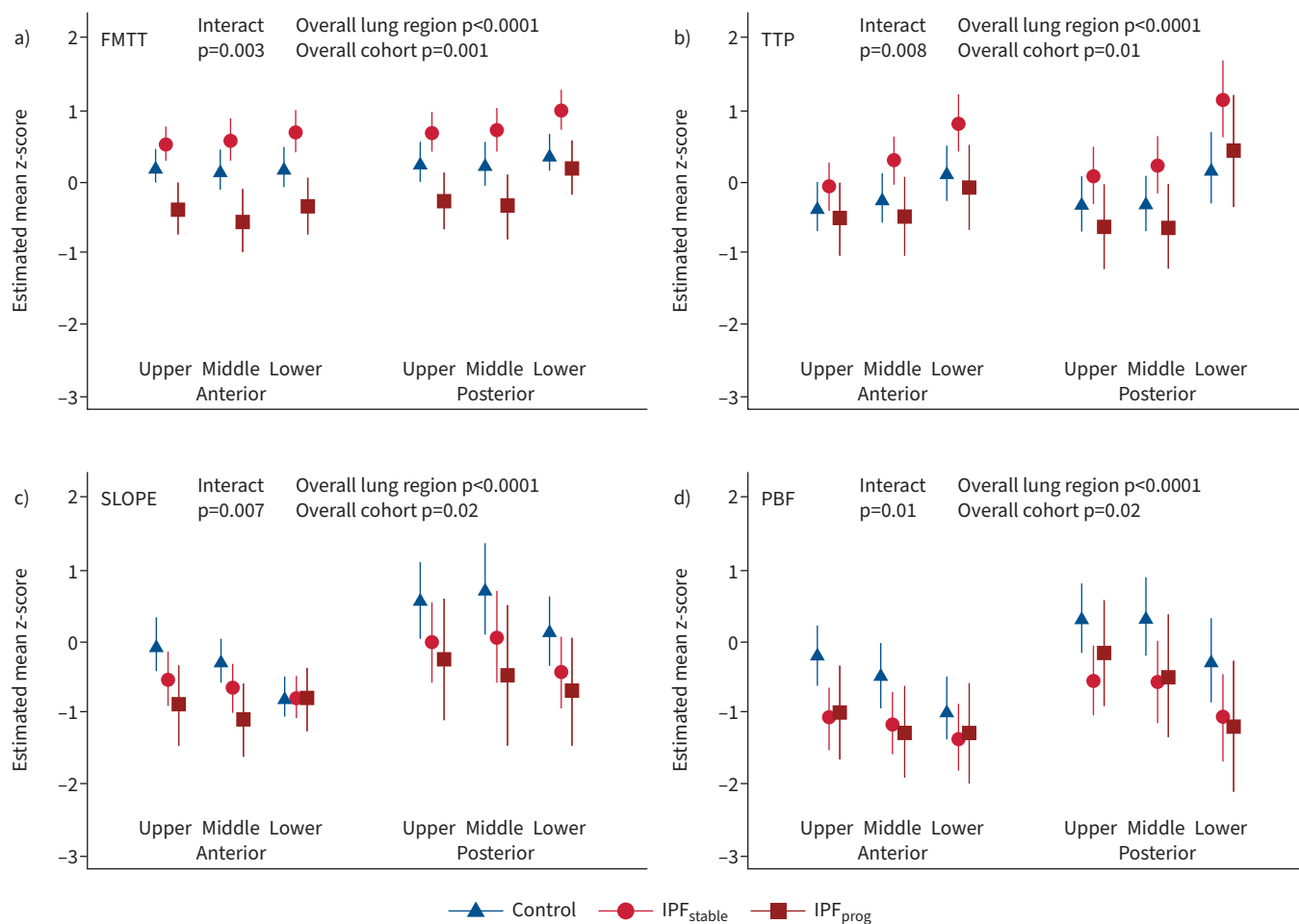
FIGURE 5 Exploratory regional repeated measure regression model results for the mean values of a) first moment transit time (FMTT), b) time to peak (TTP), c) contrast uptake slope (SLOPE) and d) pulmonary blood flow (PBF) in healthy control, stable (IPF$_{stable}$) and progressive (IPF$_{prog}$) idiopathic pulmonary fibrosis subjects.

Some clarifications should be made with respect to previous work. WEATHERLY *et al.* [14] show significant longitudinal increases in global FWHM over 6 months in IPF subjects. In this work we focus on establishing baseline differences between a healthy cohort and IPF subjects with clinical outcomes of progression after 1 year. Given our focus on clinical progression, these results are not mutually exclusive and evaluate different aspects of DCE measures in the context of IPF. The present work demonstrates improved discriminatory power by leveraging the regional information contained within DCE-MRI and we expect that this improvement will translate to longitudinal monitoring of DCE measures in IPF as well. We also note that WEATHERLY *et al.* [14] demonstrated a nonstatistically significant increase in FWHM in a small subset of nonsurvivors. This is partly in contrast to our findings, which indicate a decrease in FMTT using a different definition of progression. We suspect that the results are not directly comparable due to the different classification of "progressors" *versus* "nonsurvivors" as well as inherent differences between FWHM and FMTT as measures of transit time.

Finally, when comparing global PFT measures, FVC % pred, D_{LCO} % pred and LCI % pred all show significant differences across groups, specifically between control and IPF$_{prog}$. Of the perfusion measures, only FMTT demonstrated significant global differences. This suggests that either global perfusion measures are not as sensitive as FVC % pred, D_{LCO} % pred and LCI % pred or that global perfusion measures are measuring fundamentally different aspects of the disease. However, we emphasise that, unlike global measures of either perfusion or PFTs, regional FMTT uniquely distinguished between stable IPF and IPF progression.
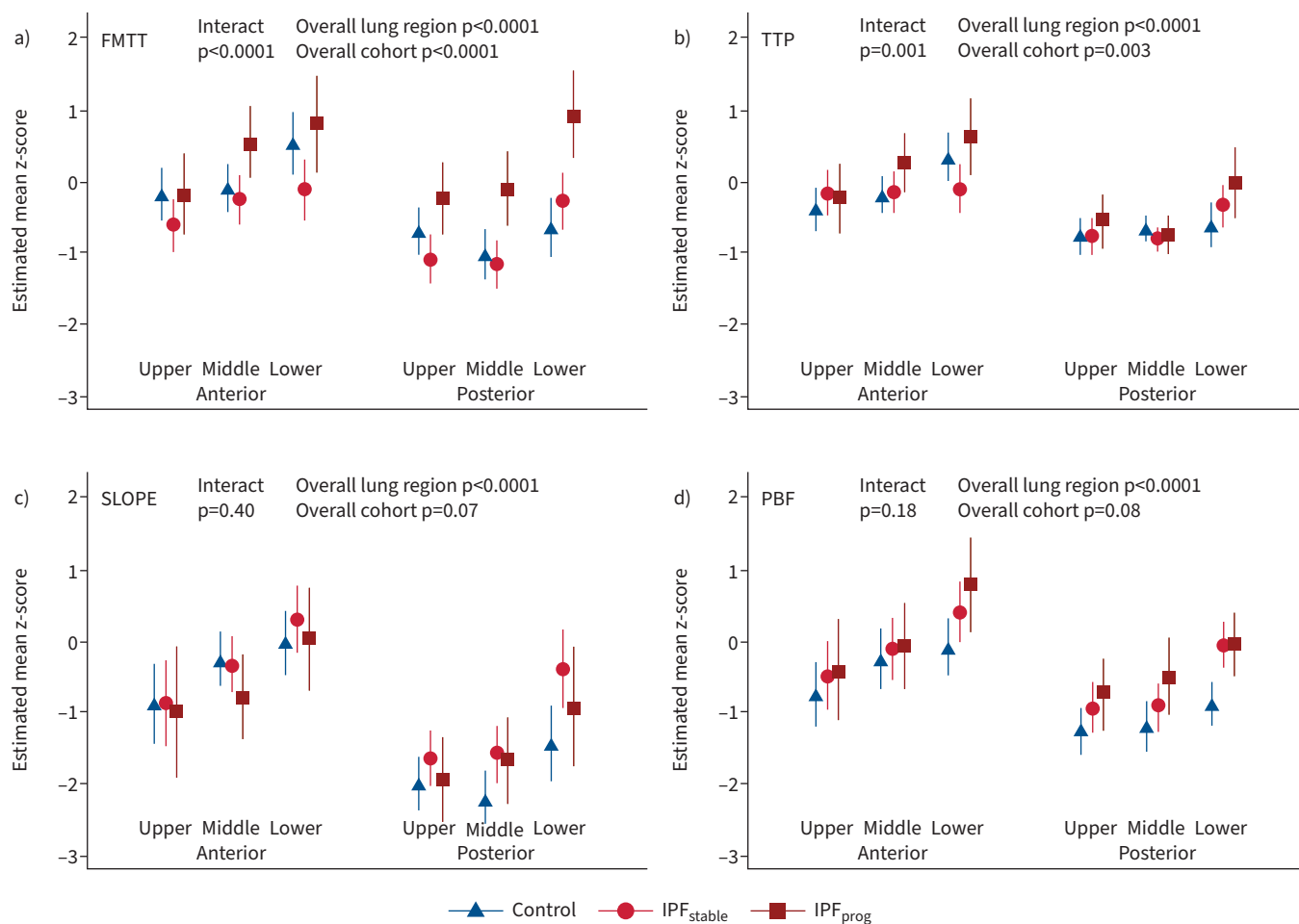
FIGURE 6 Exploratory regional repeated measure model results for the coefficients of variation of a) first moment transit time (FMTT), b) time to peak (TTP), c) contrast uptake slope (SLOPE) and d) pulmonary blood flow (PBF) in healthy control, stable (IPF$_{stable}$) and progressive (IPF$_{prog}$) idiopathic pulmonary fibrosis subjects.

Limitations

This study has some limitations. First is the small sample size, especially in the IPF$_{prog}$ subgroup, that necessarily makes the exploration of perfusion markers of progression speculative and prone to selection bias. In this study we also had an unbalanced dataset with respect to age, sex and field strength. Our cohorts have statistically different age distributions, which could affect our measures as perfusion tends to decrease with increased age. With respect to field strength differences, tissue T1 relaxation times will be longer at 3 T than at 1.5 T, which will also systematically reduce the signal-to-noise ratio in our measurements. Although our models account for these biases and imbalances it is possible that bias remains even after statistical adjustments due to insufficient overlap between groups.

Second, although we use a small, optimised, contrast dose to target the pseudo-linear relationship between contrast dose and signal amplitude, it is possible to have systematic biases in our quantitative parameters due to this signal saturation effect. We did not observe any noticeable saturation effects, and our estimates are comparable to those found in the literature for haemodynamics measured using DCE-MRI and SPECT (single-photon emission CT)/positron emission tomography.

Conclusions

In this work we demonstrate that global analysis obscures regional changes in pulmonary haemodynamics in IPF using DCE-MRI. Quantitative PBF and semiquantitative FMTT perfusion also clearly delineated healthy subjects from IPF patients. Moreover, decreased FMTT was found in the subset of IPF patients who progressed and should be investigated further as a candidate marker for IPF progression in a larger

study population. We also observed significant correlations of CV in perfusion measures with D_{LCO} % pred and LCI % pred as surrogates for vascular heterogeneity. Notably, FVC % pred, D_{LCO} % pred and LCI % pred all demonstrated significant differences between healthy and IPF, although they did not distinguish between stable and progressive IPF. In total, these results suggest DCE-MRI is a promising tool for identifying early vascular remodelling of the capillary networks in IPF, which could serve as an early predictor of rapid progression.

References

1   Meltzer EB, Noble PW. Idiopathic pulmonary fibrosis. *Orphanet J Rare Dis* 2008; 3: 8.

2   du Bois RM, Weycker D, Albera C, *et al.* Forced vital capacity in patients with idiopathic pulmonary fibrosis: test properties and minimal clinically important difference. *Am J Respir Crit Care Med* 2011; 184: 1382–1389.

3   Doubková M, Švancara J, Svoboda M, *et al.* EMPIRE Registry, Czech part: impact of demographics, pulmonary function and HRCT on survival and clinical course in idiopathic pulmonary fibrosis. *Clin Respir J* 2018; 12: 1526–1535.

4   Davies JC, Cunningham S, Alton EWFW, *et al.* Lung clearance index in CF: a sensitive marker of lung disease severity. *Thorax* 2008; 63: 96–97.

5   Torres L, Kammerman J, Hahn AD, *et al.* Structure-function imaging of lung disease using ultrashort echo time MRI. *Acad Radiol* 2019; 26: 431–441.

6   Barton GP, Torres LA, Goss KN, *et al.* Pulmonary microvascular – changes in adult survivors of prematurity: utility of DCE MRI. *Am J Respir Crit Care Med* 2020; 202: 1471–1473.

7   Maxien D, Ingrisch M, Meinel F, *et al.* Quantification of pulmonary perfusion with free-breathing dynamic contrast-enhanced MRI – a pilot study in healthy volunteers. *RöFo* 2013; 185: 1175–1181.

8   Ley S, Ley-Zaporozhan J. Pulmonary perfusion imaging using MRI: clinical application. *Insights Imaging* 2011; 3: 61–71.

9   Ohno Y, Koyama H, Matsumoto K, *et al.* Dynamic MR perfusion imaging: capability for quantitative assessment of disease extent and prediction of outcome for patients with acute pulmonary thromboembolism. *J Magn Reson Imaging* 2010; 31: 1081–1090.

10 Hueper K, Parikh M, Prince MR, *et al.* Quantitative and semi-quantitative measures of regional pulmonary parenchymal perfusion by magnetic resonance imaging and their relationships to global lung perfusion and lung diffusing capacity – the MESA COPD Study. *Invest Radiol* 2013; 48: 223–230.

11 Sergiacomi G, Bolacchi F, Cadioli M, *et al.* Combined pulmonary fibrosis and emphysema: 3D time-resolved MR angiographic evaluation of pulmonary arterial mean transit time and time to peak enhancement. *Radiology* 2010; 254: 601–608.

12 Mirsadraee S, Tse M, Kershaw L, *et al.* T1 characteristics of interstitial pulmonary fibrosis on 3 T MRI – a predictor of early interstitial change? *Quant Imaging Med Surg* 2016; 6: 42–49.

13 Lavelle LP, Brady D, McEvoy S, *et al.* Pulmonary fibrosis: tissue characterization using late-enhanced MRI compared with unenhanced anatomic high-resolution CT. *Diagn Interv Radiol* 2017; 23: 106–111.

14 Weatherley ND, Eaden JA, Hughes PJC, *et al.* Quantification of pulmonary perfusion in idiopathic pulmonary fibrosis with first pass dynamic contrast-enhanced perfusion MRI. *Thorax* 2021; 76: 144–151.

15 Montesi S, Zhou IY, Digumarthy S, *et al.* Dynamic contrast-enhanced MRI to assess the microvasculature in IPF. *Chest* 2019; 156: 4 Suppl., A2268.

16 Meier P, Zierler KL. On the theory of the indicator-dilution method for measurement of blood flow and volume. *J Appl Physiol* 1954; 6: 731–744.

17 Ohno Y, Hatabu H, Murase K, *et al.* Quantitative assessment of regional pulmonary perfusion in the entire lung using three-dimensional ultrafast dynamic contrast-enhanced magnetic resonance imaging: preliminary experience in 40 subjects. *J Magn Reson Imaging* 2004; 20: 353–365.

18 Hopkins SR, Levin DL, Emami K, *et al.* Advances in magnetic resonance imaging of lung physiology. *J Appl Physiol* 2007; 102: 1244–1254.

19   Østergaard L, Weisskoff RM, Chesler DA, *et al.* High resolution measurement of cerebral blood flow using intravascular tracer bolus passages. Part I: mathematical approach and statistical analysis. *Magn Reson Med* 1996; 36: 715–725.

20   Neeb D, Kunz RP, Ley S, *et al.* Quantification of pulmonary blood flow (PBF): validation of perfusion MRI and nonlinear contrast agent (CA) dose correction with $H_2^{15}O$ positron emission tomography (PET). *Magn Reson Med* 2009; 62: 476–487.

21   Wang K, Schiebler ML, Francois CJ, *et al.* Pulmonary perfusion MRI using interleaved variable density sampling and HighlY constrained Cartesian reconstruction (HYCR): pulmonary perfusion using IVD HYCR. *J Magn Reson Imaging* 2013; 38: 751–756.

22   Saranathan M, Rettmann DW, Hargreaves BA, *et al.* DIfferential Subsampling with Cartesian Ordering (DISCO): a high spatio-temporal resolution Dixon imaging sequence for multiphasic contrast enhanced abdominal imaging. *J Magn Reson Imaging* 2012; 35: 1484–1492.

23   Yushkevich PA, Piven J, Hazlett HC, *et al.* User-guided 3D active contour segmentation of anatomical structures: significantly improved efficiency and reliability. *NeuroImage* 2006; 31: 1116–1128.

24   Kohlmann P, Strehlow J, Jobst B, *et al.* Automatic lung segmentation method for MRI-based lung perfusion studies of patients with chronic obstructive pulmonary disease. *Int J Comput Assist Radiol Surg* 2015; 10: 403–417.

25   Kohlmann P, Laue H, Krass S, *et al.* Fully-automatic determination of the arterial input function for dynamic contrast-enhanced pulmonary MR imaging. 2011. www.bmva.org/miua/2011/miua-11-43.pdf Date last accessed: 11 March 2022.

26   Risse F, Kuder TA, Kauczor H-U, *et al.* Suppression of pulmonary vasculature in lung perfusion MRI using correlation analysis. *Eur Radiol* 2009; 19: 2569–2575.

27   Stanojevic S, Grham B, Cooper B, *et al.* Global lung function initiative: reference equations for the transfer factor for carbon monoxide (T_{LCO}). *Eur Respir J* 2016; 48: Suppl. 60, OA283.

28   Østergaard L. Principles of cerebral perfusion imaging by bolus tracking. *J Magn Reson Imaging* 2005; 22: 710–717.

29   Sourbron S, Luypaert R, Morhard D, *et al.* Deconvolution of bolus-tracking data: a comparison of discretization methods. *Phys Med Biol* 2007; 52: 6761–6778.

30   Bell LC, Wang K, Del Rio AM, *et al.* Comparison of models and contrast agents for improved signal and signal linearity in dynamic contrast-enhanced pulmonary MRI. *Invest Radiol* 2015; 50: 174–178.

31   Ebina M. Pathognomonic remodeling of blood and lymphatic capillaries in idiopathic pulmonary fibrosis. *Respir Investig* 2017; 55: 2–9.

32   Ebina M, Shimizukawa M, Shibata N, *et al.* Heterogeneous increase in CD34-positive alveolar capillaries in idiopathic pulmonary fibrosis. *Am J Respir Crit Care Med* 2004; 169: 1203–1208.

33   Mlika M, Bacha S, Braham E, *et al.* The inter-connection between fibrosis and microvascular remodeling in idiopathic pulmonary fibrosis: reality or just a phenomenon. *Respir Med Case Rep* 2016; 17: 30–33.

34   Farkas L, Kolb M. Pulmonary microcirculation in interstitial lung disease. *Proc Am Thorac Soc* 2011; 8: 516–521.

35   Levin DL, Chen Q, Zhang M, *et al.* Evaluation of regional pulmonary perfusion using ultrafast magnetic resonance imaging. *Magn Reson Med* 2001; 46: 166–171.

36   Plantier L, Cazes A, Dinh-Xuan A-T, *et al.* Physiology of the lung in idiopathic pulmonary fibrosis. *Eur Respir Rev* 2018; 27: 170062.

37   Lederer DJ, Martinez FJ. Idiopathic pulmonary fibrosis. *N Engl J Med* 2018; 378: 1811–1823.

38   Jacob J, Bartholmai BJ, Rajagopalan S, *et al.* Mortality prediction in idiopathic pulmonary fibrosis: evaluation of computer-based CT analysis with conventional severity measures. *Eur Respir J* 2017; 49: 1601011.

39   Parra ER, David YR, da Costa LRS, *et al.* Heterogeneous remodeling of lung vessels in idiopathic pulmonary fibrosis. *Lung* 2005; 183: 291–300.

40   Puxeddu E, Cavalli F, Pezzuto G, *et al.* Impact of pulmonary vascular volume on mortality in IPF: is it time to reconsider the role of vasculature in disease pathogenesis and progression? *Eur Respir J* 2017; 49: 1602345.

41   Probst CK, Montesi SB, Medoff BD, *et al.* Vascular permeability in the fibrotic lung. *Eur Respir J* 2020; 56: 1900100.